




AlphaFold2-aware protein–DNA binding site prediction using graph transformer

Qianmu Yuan , Sheng Chen, Jiahua Rao , Shuangjia Zheng , Huiying Zhao and Yuedong Yang

Corresponding author: Yuedong Yang, School of Computer Science and Engineering, Sun Yat-sen University, Guangzhou 510000, China, and Key Laboratory of Machine Intelligence and Advanced Computing of MOE, Sun Yat-sen University, Guangzhou 510000, China. Tel.: +86 020-37106046; Fax: +86 020-37106020. E-mail: yangyd25@mail.sysu.edu.cn

Abstract

Protein–DNA interactions play crucial roles in the biological systems, and identifying protein–DNA binding sites is the first step for mechanistic understanding of various biological activities (such as transcription and repair) and designing novel drugs. How to accurately identify DNA-binding residues from only protein sequence remains a challenging task. Currently, most existing sequence-based methods only consider contextual features of the sequential neighbors, which are limited to capture spatial information. Based on the recent breakthrough in protein structure prediction by AlphaFold2, we propose an accurate predictor, GraphSite, for identifying DNA-binding residues based on the structural models predicted by AlphaFold2. Here, we convert the binding site prediction problem into a graph node classification task and employ a transformer-based variant model to take the protein structural information into account. By leveraging predicted protein structures and graph transformer, GraphSite substantially improves over the latest sequence-based and structure-based methods. The algorithm is further confirmed on the independent test set of 181 proteins, where GraphSite surpasses the state-of-the-art structure-based method by 16.4% in area under the precision-recall curve and 11.2% in Matthews correlation coefficient, respectively. We provide the datasets, the predicted structures and the source codes along with the pre-trained models of GraphSite at <https://github.com/biomed-AI/GraphSite>. The GraphSite web server is freely available at <https://biomed.nsc-cg.cn/apps/GraphSite>.

Keywords: protein–DNA binding site, AlphaFold2, predicted protein structure, graph transformer

Introduction

Protein–DNA interactions play crucial roles in many biological processes such as transcription, repair and signal transduction [1, 2]. Although protein–DNA binding affinity prediction [3, 4], protein-interacting site prediction on DNA (e.g. promoter prediction; [5]) and protein–DNA docking [6] have been widely studied, accurately identifying amino acids involved in protein–DNA interactions solely based on proteins is also an important topic in bioinformatics, which helps to improve molecular docking [7, 8], understand disease mechanism [9, 10], predict protein function [11, 12] and identify potential drug target for novel drug design [13, 14]. However, conventional experimental methods for DNA-binding site detection such as X-ray crystallography [15] and fast ChIP [16] are costly and time-consuming. Although protein–DNA

binding patterns are complicated and many proteins may specifically recognize local DNA structures such as hairpins, cruciforms and G-quadruplexes [17, 18], DNA-binding residues are often conserved [19]. Therefore, it is necessary and feasible to develop complementary computational methods capable of making reliable and accurate DNA-binding site prediction.

Computational methods for DNA-binding site prediction can be classified into two classes, sequence-based and structure-based methods, according to their used information. Sequence-based methods such as DNAPred [20], DNAGenie [21] and NCBRPred [22] learn local patterns of DNA-binding characteristics through sequence-derived features. For example, NCBRPred adopts evolutionary conservative information and predicted secondary structure and solvent accessibility extracted from

Qianmu Yuan is a PhD student in the School of Computer Science and Engineering at Sun Yat-Sen University. His research interests lie in deep learning, graph neural network, protein structure prediction and protein function prediction.

Sheng Chen is a PhD student in the School of Computer Science and Engineering at Sun Yat-Sen University. His research interests include deep learning, protein design, protein structure prediction and graph neural network.

Jiahua Rao is a PhD student in the School of Computer Science and Engineering at Sun Yat-Sen University. His research interests include deep learning, multi-omics integration, knowledge graph, and computational biology. This work is done when he works as an intern in Galixir Technologies Ltd, Beijing, China.

Shuangjia Zheng is a PhD student in the School of Computer Science and Engineering at Sun Yat-Sen University. His research interests lie in deep learning, knowledge graph, drug discovery, and computational biology. He worked directly or indirectly for Galixir during the course of this work.

Huiying Zhao is an associate research fellow in the Sun Yat-sen Memorial Hospital at Sun Yat-sen University. Her research interests include pathogenic gene analysis, protein function and RNA function prediction.

Yuedong Yang is a professor in the School of Computer Science and Engineering and the National Super Computer Center at Guangzhou, Sun Yat-sen University, China. His research group emphasizes on developing HPC and AI algorithms for protein function prediction, multi-omics data integration and intelligent drug design. He is also responsible for constructing the HPC platform for biomedical applications based on the Tianhe-2 supercomputer.

Received: October 9, 2021. **Revised:** November 24, 2021. **Accepted:** December 9, 2021

© The Author(s) 2022. Published by Oxford University Press. All rights reserved. For Permissions, please email: journals.permissions@oup.com

protein sequence and employs bidirectional Gated Recurrent Units to learn local patterns from sequence contexts using sliding-window strategy. Although these sequence-based approaches require protein sequences only, the lacks of using tertiary structures cause their limited predictive accuracies.

By comparison, structure-based approaches inferring binding sites from known structures are often more accurate, which can be generally categorized into template-based methods, machine learning based methods and hybrid methods. Template-based methods identify DNA-binding sites using the sequence and structure information of templates, which are selected by alignment or comparison algorithms [23, 24]. Nevertheless, for the proteins that have no high-quality template, the performance of these methods will be seriously restricted. With features derived from protein structures, recent structure-based machine learning methods represent protein structures as voxels in three-dimensional Euclidean space or nodes in connected graphs. For example, DeepSite [25] maps protein atoms into 3D voxels and employs 3D convolutional neural networks (3DCNN) to extract features from neighborhood of the target residue. Alternately, GraphBind [26] encodes protein structures as graphs and adopts graph neural networks (GNN) to learn the local tertiary patterns for binding residue prediction. Hybrid methods integrate template-based methods and machine learning based methods simultaneously, such as DNABind [27], COACH-D [28] and NucBind [7]. Albeit powerful, the structure-based methods are not applicable to most proteins that do not have known tertiary structures due to the difficulties to determine protein structures experimentally [29].

With the development of deep learning techniques, protein structure prediction is experiencing a breakthrough. The representative method, AlphaFold2 [30], has incorporated physical and biological knowledge about protein structure, information of multi-sequence alignment (MSA) and the sophisticated design of the deep learning algorithm. The method was shown able to predict protein structure with atomic accuracy even when no similar structure template is known, and demonstrated accuracy competitive with experiment in a majority of cases in the challenging 14th Critical Assessment of protein Structure Prediction (CASP14). Such breakthrough will undoubtedly benefit downstream protein function studies, including binding site prediction.

Effective learning of protein structure remains a challenging task, even though 1DCNN [31], 2DCNN [32], 3DCNN [33], GNN and its variants [34, 35] have been widely adopted. On the other hand, transformer [36] is well-acknowledged as the most powerful neural network in modelling sequential data, such as natural language [37], drug SMILES [38] and protein sequence [39]. In the last few years, transformer variants have also been shown great performance in graph representation

learning [40–42]. Therefore, it is promising to advance the protein binding site prediction by constructing accurate structure model from sequence and effectively learning the structural information through the recent graph transformer technique.

In this study, we have developed a novel method GraphSite, which applies graph transformer network and predicted protein structures from AlphaFold2 for sequence-based prediction of DNA-binding residues. Specifically, we integrate MSA and structural information to construct residual features and calculate pairwise amino acid distances to mask out the spatially remote amino acids when calculating attention scores in the transformer. With the spatial information and structure-aware transformer, GraphSite was found to outperform other sequence-based and structure-based methods through various performance evaluations. To the best of our knowledge, this is the first work that utilizes AlphaFold2-predicted structures and graph transformer for protein–DNA binding site prediction, which can be easily extended to sequence-based prediction of other functional sites.

Materials and methods

Datasets

We adopted two publicly available benchmark datasets from the previous study [26] to train and test our method: Train_573 and Test_129, which are named by the numbers of proteins in the datasets. These two datasets were collected from the BioLiP database [43], which pre-computes binding sites according to experimentally determined complex structures from Protein Data Bank (PDB; [44]). Concretely, Train_573 contains proteins released before 6 January 2016 while Test_129 from 6 January 2016 to 5 December 2018. In these datasets, a DNA-binding residue was defined if the smallest atomic distance between the target residue and the DNA molecule is less than 0.5 Å plus the sum of the Van der Waal's radius of the two nearest atoms. To deal with the data imbalance problem, the authors [26] applied data augmentation on Train_573, which transferred binding annotations from protein chains with similar sequences (sequence identity >0.8) and structures (TM scores >0.5) to increase the number of binding residues. This was conducted for the following reasons: (i) similar proteins, although could derived from different organisms, may have the same biological function. (ii) different resolutions or co-factors may lead to minor differences in the structures for the same protein. Finally, CD-HIT [45] was used to ensure no redundant protein with >30% sequence identity within the training set and between the training and test set. To further demonstrate the generalization of our method, we built another independent test set (Test_181) based on newly released DNA-binding proteins in BioLiP (6 December 2018–19 August 2021). We have removed redundant proteins sharing sequence identity >30% over

Table 1. Statistics of the three-benchmark datasets used in this study

Dataset	Binding residues	Non-binding residues	% of binding residues
Train_573	14 479	145 404	9.06
Test_129	2240	35 275	5.97
Test_181	3208	72 050	4.26

Note: The columns give, in order, the dataset name, the number of binding, the number of non-binding residues in each dataset, and the percentage of the binding residues out of total.

30% overlap with any sequence in the above two datasets and within Test_181 using CD-HIT. Details of the number of binding and non-binding residues of these datasets are given in Table 1.

Protein representation

In our framework, the DNA-binding site prediction task is treated as a graph node classification problem, where a protein consisting of n amino acid residues is represented by a node feature matrix X and a distance matrix D .

Predicted protein structures and distance maps

Following the tutorial at <https://github.com/deepmind/alphafold>, we downloaded the model parameters and genetic databases including UniRef90 [46], MGnify [47], BFD [48], Uniclust30 [49], PDB70 [50] and PDB [44] to implement AlphaFold2 in the Tianhe-2 supercomputer. We set the ‘-max_template_date’ parameter to 14 May 2020 just as the AlphaFold2 model in CASP14 to predict the protein structures in Train_573 and Test_129, from which the relaxed models with the highest confidences (measured by the predicted local distance difference test (LDDT) scores) were chosen. However, to further avoid the possibility that AlphaFold2 might use the native known structures in PDB as templates, we set ‘-max_template_date’ to 5 December 2018 when predicting proteins in the independent Test_181. This made Test_181 more challenging and closer to the situation where only protein sequences instead of similar templates are available. According to the predicted protein structural models from AlphaFold2, we acquired the coordinate of the $C\alpha$ atom of each amino acid residue, and then calculated the Euclidean distances between all residue pairs, which formed a distance map $D \in \mathbb{R}^{n \times n}$.

Node features

We employed two groups of amino acid features to train our model: MSA information and structural properties, which were concatenated and formed the final node feature matrix $X \in \mathbb{R}^{n \times 438}$ with n denoting the length of a protein sequence.

MSA information

Co-evolving amino acids may structurally contact, and evolutionarily conserved residues may contain motifs related to important protein properties such as

DNA-binding propensity. Here, we employed the ‘single representation’ feature output by AlphaFold2 along with the predicted structures. This single representation is derived by a linear projection of the first row of the MSA representation, which is a highly processed MSA feature matrix through 48 Evoformer blocks in AlphaFold2. In addition, we also explored the widely used position-specific scoring matrix (PSSM) and hidden Markov models (HMM) profile. Concretely, PSSM was generated by running PSI-BLAST [51] to search the query sequence against UniRef90 database with three iterations and an E-value of 0.001. The HMM profile was produced by running HHblits [52] to align the query sequence against UniClust30 database with default parameters. Each amino acid was encoded into a 384-dimensional vector in single representation and 20-dimensional vector in PSSM or HMM, and the values were normalized to scores between 0 and 1 using Equation (1), where v is the original feature value, and Min and Max are the smallest and biggest values of this feature type observed in the training set.

$$v_{\text{norm}} = \frac{v - \text{Min}}{\text{Max} - \text{Min}} \quad (1)$$

Structural properties

Three types of structural properties were extracted by the program DSSP [53] using predicted structures: (i) nine-dimensional one-hot secondary structure profile where the first eight dimensions represent eight-secondary structure states, and the last dimension represents unknown secondary structure. (ii) Peptide backbone torsion angles PHI and PSI, which were converted to a four-dimensional feature vector using sine and cosine transformations. (iii) Solvent accessible surface area (ASA), which was normalized to relative solvent accessibility (RSA) by the maximal possible ASA of the corresponding amino acid type. This 14-dimensional structural feature group is named DSSP in this article.

The architecture of GraphSite

Figure 1 shows the overall architecture of the proposed framework GraphSite, where the protein sequence is input to AlphaFold2 to produce the single representation and the predicted protein structure, from which the distance map and DSSP are extracted. Finally, the single representation, DSSP and sequence-derived features PSSM and HMM are concatenated to form the node feature vector, which is then input to the graph transformer masked by the distance map to learn the DNA-binding site patterns.

Graph transformer

The traditional transformer encoder layer consists of a multi-head self-attention module and a position-wise

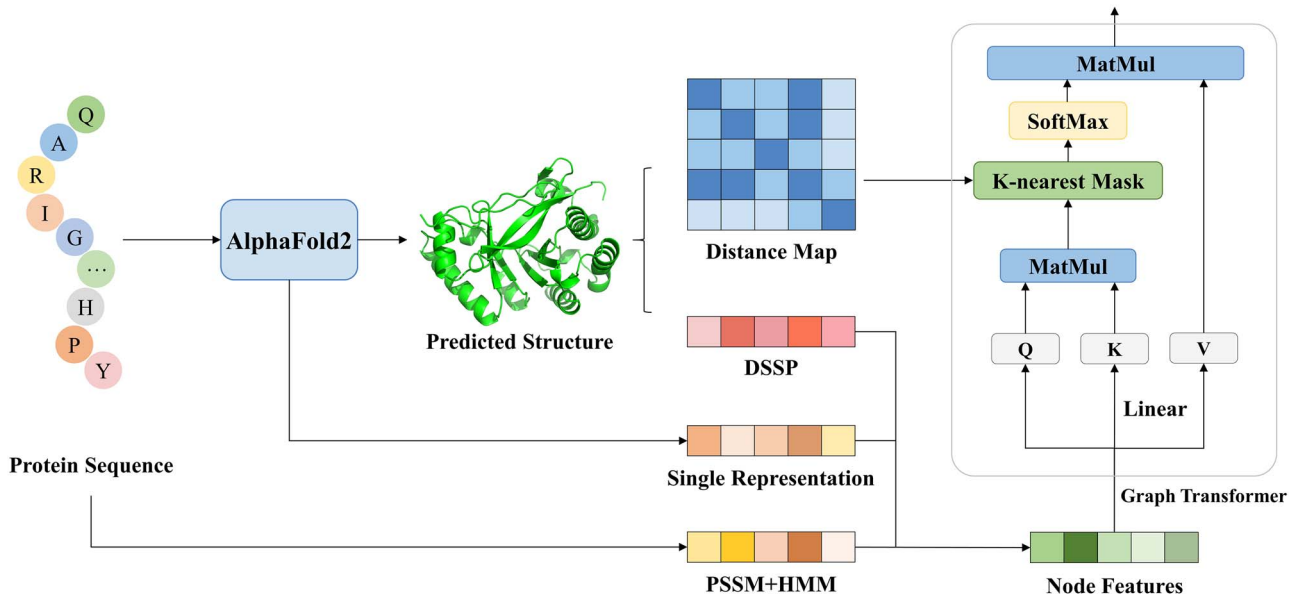


Figure 1. The overall architecture of GraphSite. The protein sequence is input to AlphaFold2 to produce the single representation and the predicted protein structure, from which the distance map and DSSP are extracted. Then, the single representation, DSSP and sequence-derived features PSSM and HMM are concatenated to form the node feature vector, which is then input to the graph transformer model with k -nearest mask by the distance map to learn the DNA-binding site patterns.

feed-forward network. Let $H = [h_1^T, \dots, h_n^T]^T \in \mathbb{R}^{n \times d}$ denote the input of the self-attention module where d is the hidden dimension and $h_i \in \mathbb{R}^{1 \times d}$ is the hidden representation of the i th amino acid. Note that the initial $H^{(0)}$ does not have to be the feature matrix X , which means that a fully connected layer can be applied on X to obtain the initial hidden representation $H^{(0)}$. The input $H^{(l)}$ is projected by three matrices $W_Q \in \mathbb{R}^{d \times d_K}$, $W_K \in \mathbb{R}^{d \times d_K}$ and $W_V \in \mathbb{R}^{d \times d_V}$ to the corresponding queries, keys and values representation Q, K, V :

$$Q = H^{(l)}W_Q, K = H^{(l)}W_K, V = H^{(l)}W_V \quad (2)$$

The self-attention is then calculated as:

$$A = \frac{QK^T}{\sqrt{d_K}} \quad (3)$$

$$H^{(l+1)} = \text{Attn}(H^{(l)}) = \text{softmax}(A)V \quad (4)$$

where A is a matrix capturing the similarities between queries and keys. In order to take the protein structure information into account for focusing on spatially adjacent residues, we adopt k -nearest mask according to the distance matrix D to mask out the spatially remote amino acids, which means that for node i , only spatially adjacent nodes $j \in \text{Neighbor}(i, k)$ are used to calculate the attention scores in the transformer. In order to jointly attend to information from different representation subspaces at different positions, we use multi-head attention to linearly project the queries, keys and values h times, perform the attention function in parallel and finally concatenate them together. In this study, $d_K = d_V = d/h$.

Multilayer perceptron

The output of the last graph transformer layer is input to the multilayer perceptron (MLP) to predict the DNA-binding probabilities of all n amino acid residues:

$$Y' = \text{Sigmoid}(H^{(L)}W + b) \quad (5)$$

where $H^{(L)} \in \mathbb{R}^{n \times d}$ is the output of the L th graph transformer layer; $W \in \mathbb{R}^{d \times 1}$ is the weight matrix; $b \in \mathbb{R}$ is the bias term and $Y' \in \mathbb{R}^{n \times 1}$ is the predictions of n amino acid residues. The sigmoid function normalizes the output of the network into binding probabilities ranging from 0 to 1.

Implementation details

We performed 5-fold cross-validation (CV) on the training data, where the data were split into 5-folds randomly. Each time, a model was trained on 4-folds and evaluated on the remaining one fold. This process was repeated five times and the performances on the 5-folds were averaged as the overall validation performance, which was used to choose the best feature combination and optimize all hyperparameters through grid search (Supplementary Table S1). In the testing phase, all five-trained models in the CV were used to make predictions, which were averaged as the final predictions of our method.

Specifically, we utilized a 2-layer graph transformer module with 64 hidden units and the following set of hyperparameters: $h=4$, $k=30$ and batch size of 16. We employed the Adam optimizer [54] with $\beta_1=0.9$, $\beta_2=0.99$, $\varepsilon=10^{-5}$, weight decay of 10^{-5} and learning rate of 3×10^{-4} for model optimization on the binary cross entropy loss. The dropout rate was set to 0.2 to avoid overfitting. We implemented the proposed model with Pytorch 1.7.1

[55]. Within each epoch, we drew 5000 samples from the training data using random sampling with replacement to train our model. The training process lasted at most 15 epochs and we performed early-stopping with patience of 4 epochs based on the validation performance, which took ~40 min on an Nvidia GeForce RTX 3090 GPU. In the testing phase, it took ~5 s to make prediction for one protein with pre-computed features.

Evaluation metrics

Similar to the previous studies [56, 57], we used specificity (Spe), precision (Pre), recall (Rec), F1-score (F1), Matthews correlation coefficient (MCC), area under the receiver operating characteristic curve (AUC) and area under the precision-recall curve (AUPR) to measure the predictive performance:

$$\text{Spe} = \frac{\text{TN}}{\text{TN} + \text{FP}} \quad (6)$$

$$\text{Pre} = \frac{\text{TP}}{\text{TP} + \text{FP}} \quad (7)$$

$$\text{Rec} = \frac{\text{TP}}{\text{TP} + \text{FN}} \quad (8)$$

$$\text{F1} = 2 \times \frac{\text{Precision} \times \text{Recall}}{\text{Precision} + \text{Recall}} \quad (9)$$

$$\text{MCC} = \frac{\text{TP} \times \text{TN} - \text{FN} \times \text{FP}}{\sqrt{(\text{TP} + \text{FP}) \times (\text{TP} + \text{FN}) \times (\text{TN} + \text{FP}) \times (\text{TN} + \text{FN})}} \quad (10)$$

where true positives (TP) and true negatives (TN) denote the number of binding and non-binding sites identified correctly, and false positives (FP) and false negatives (FN) denote the number of incorrectly predicted binding and non-binding sites, respectively. AUC and AUPR are independent of thresholds, thus revealing the overall performance of a model. The other metrics were calculated using a threshold to convert the predicted binding probabilities to binary predictions, which was determined by maximizing F1-score for the model. We used AUPR for the above hyperparameter selection as it is more sensitive and it emphasizes more on the minority class in imbalanced two-class classification tasks [58].

Significance tests were performed to investigate if the results are not biased by a subset of test proteins by measuring whether the predictive performance is consistent over different subsets. Similar to [26, 59], we randomly sampled 70% of the test proteins and calculated the AUPRs of the best-performing method and other methods. This was repeated 10 times and we compared the corresponding 10 paired results. If the measurements were normal, as tested by the Anderson–Darling test [60] with 0.05 significance, we applied the paired t-test to investigate significance. Otherwise, the Wilcoxon rank sum test [61] was utilized. If P -value < 0.05 , the difference between a given pair of methods is considered statistically significant.

Results

Performance on the 5-fold CV and independent tests

We evaluated the performance of GraphSite by AUC and AUPR using 5-fold CV on the Train_573 dataset and independent tests on the Test_129 and Test_181 datasets. The final GraphSite model obtains AUC of 0.915, 0.934 and 0.917; as well as AUPR of 0.589, 0.544 and 0.369 on the 5-fold CV and two independent tests, respectively. The consistent AUC on the CV and tests indicate the robustness of our model. Note that the AUPR drops ~0.18 in Test_181, which might be ascribed to the lower positive sample ratio, or the lower predicted qualities of the protein structures in this dataset (discussed in Section ‘Impact of the quality of predicted protein structure’). Since the prediction of GraphSite is the average predictive scores from the five-trained models in CV, we also discussed the uncertainty of our method, which is empirically measured by the standard deviation of these five scores. As shown in [Supplementary Table S2](#), the predictions are more accurate when GraphSite is more confident and vice versa.

In order to demonstrate the advantages of protein geometric knowledge and the graph transformer model, we compared GraphSite with a baseline method BiLSTM, which contains a two-layer bidirectional long short-term memory network with 256 hidden units and an MLP module. This model uses the same residue features as GraphSite and serves as a geometric-agnostic baseline to evaluate the impact of the spatial information for binding residue prediction. As shown in [Supplementary Table S3](#), GraphSite yields higher F1, MCC, AUC and AUPR values, which are 0.064(0.051), 0.068(0.054), 0.021(0.036) and 0.073(0.073) higher than those of BiLSTM on Test_129(Test_181), respectively. [Figure 2](#) and [Supplementary Figure S1](#) show the precision-recall curves and ROC curves of GraphSite and BiLSTM on the CV, Test_129 and Test_181, where the curves of GraphSite are largely located above those of BiLSTM. Here, the k -nearest mask helps GraphSite focus on the spatially adjacent residues, whereas remote residues can still be learned since the whole graph is connected. As shown in [Supplementary Table S4](#), removal of the k -nearest mask leads to AUPR drops (0.036 and 0.034) on both Test_129 and Test_181.

The performance improvement of GraphSite over BiLSTM is likely due to its better capability in capturing long-range contact information. To illustrate this, we compared the performance of GraphSite and BiLSTM on amino acids with different number of non-local contacts, defined as the contacts from the residues that are > 20 residues away in sequence positions, but ≤ 12 Å in terms of their atomic distances between $C\alpha$ atoms. [Figure 3](#) shows that GraphSite consistently surpasses BiLSTM on Test_181 and more importantly, the performance gap between them enlarges as the non-local contact number of the amino acids increases. Specifically, the performance of GraphSite surpasses BiLSTM by 8.6% in MCC on

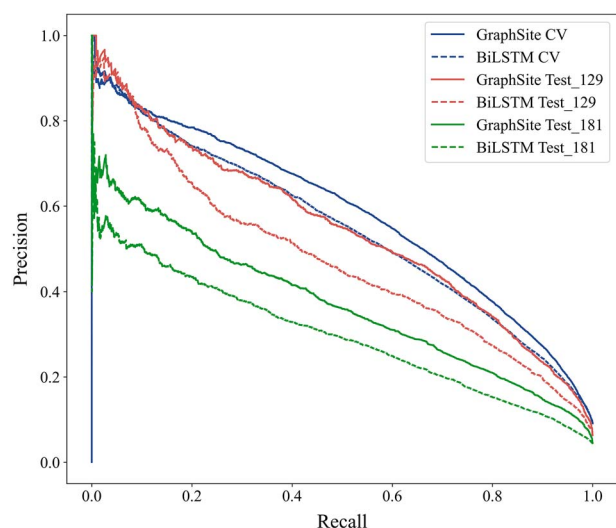


Figure 2. Precision-recall curves of GraphSite and BiLSTM on the CV, Test_129 and Test_181.

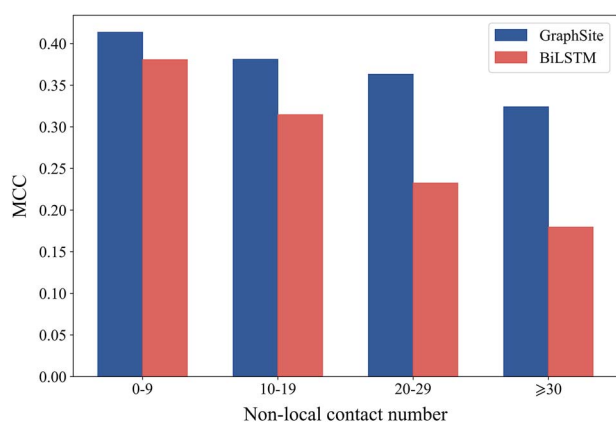


Figure 3. The MCC of GraphSite and BiLSTM on amino acids with different number of non-local contacts in Test_181.

the amino acids with 0–9 non-local contacts, and the gap widens to as much as 80.5% on the amino acids with ≥ 30 non-local contacts. Similar results can also be observed in Test_129 (Supplementary Figure S2). These comparisons highlight the importance of the spatial information, and the effectiveness of GraphSite in harnessing protein structural knowledge especially non-local contacts for DNA-binding residue recognition.

Feature importance

To demonstrate the relative importance of each feature we adopted, we conducted feature ablation experiments by using one feature individually or excluding one feature from the final feature combination. As shown in Table 2, when using single feature group as node features, the highly processed single representation from AlphaFold2 already gives satisfactory performance with AUPR of 0.520 in Test_129 and 0.336 in Test_181. On the other hand, using DSSP solely as node features yields the worst performance with AUPR of 0.126 in Test_129 and 0.080 in Test_181, indicating that structural properties of amino acids such as secondary structure and

RSA are insufficient to capture the complicated patterns of DNA-binding sites. Vice versa, the removal of single representation from the final feature combination leads to the greatest performance drops of ~ 0.1 in AUPR for the two-test sets, and the removal of DSSP leads to the smallest performance drops as expected. In addition, although both the single representation and evolutionary features (PSSM and HMM) contain MSA information, the removal of PSSM and HMM still leads to AUPR drop of 0.021 in Test_129 and 0.037 in Test_181. The performance reduction when removing any feature group suggests that the combined feature groups are nonredundant.

Comparison with state-of-the-art methods

We compared GraphSite with three sequence-based (SVMnuc, NCBRPred and DNAPred) and four structure-based (COACH-D, NucBind, DNABind and GraphBind) predictors on Test_129, where GraphSite outperforms all other methods significantly (shown in Table 3). Concretely, GraphSite surpasses the second-best sequence-based method DNAPred by 56.3% in MCC and 48.2% in AUPR, respectively. In addition, GraphSite achieves recall and precision of 0.665 and 0.460 on Test_129, respectively, surpassing all other sequence-based methods. It should be noted that recall and precision are unbalanced measures strongly depending on thresholds. Though GraphSite is a sequence-based predictor input with protein sequences only, GraphSite outperforms the latest structure-based method GraphBind by 0.020 in MCC and 0.025 in AUPR, respectively. This is reasonable because: (i) GraphBind only uses the evolutionary features PSSM and HMM from MSA, whereas our method additionally employs the informative single representation from AlphaFold2. (ii) The graph transformer model is proven to be powerful (Figure 2). (iii) The AlphaFold2-predicted protein structures used by GraphSite are of high quality (discussed in Section ‘Impact of the quality of predicted protein structure’). On the other hand, the performance of these four structure-based methods will further decrease when using predicted structures as input (e.g. AUPR from 0.519 to 0.497 for GraphBind), and the superiority of our method will be further reflected. Besides, we also tested GraphSite using the native structures as input, which will cause performance drop of AUPR from 0.544 to 0.502, since our method were trained using predicted structures. However, re-training the model using native structures will restore the AUPR to a similar level (0.541) as before.

To further demonstrate the generalization and stability of our method, we also compared GraphSite with other methods on our newly built independent Test_181. Note that this is a more challenging dataset for our method since we set ‘–max_template_date’ in AlphaFold2 before the release dates of all proteins in Test_181. As shown in Table 3, the performance ranks of these methods are generally consistent as in Test_129, and GraphSite still outperforms all other methods significantly, including the structure-based methods

Table 2. The AUC and AUPR of the 5-fold CV, Test_129 and Test_181 using a single feature individually or excluding each feature in turn from the final feature combination

Feature	CV AUC	CV AUPR	Test_129 AUC	Test_129 AUPR	Test_181 AUC	Test_181 AUPR
AF2 Single	0.906	0.557	0.925	0.520	0.908	0.336
Evo	0.864	0.417	0.888	0.381	0.854	0.232
DSSP	0.691	0.173	0.721	0.126	0.686	0.080
-AF2 Single	0.886	0.497	0.913	0.452	0.882	0.263
-Evo	0.911	0.568	0.928	0.523	0.909	0.332
-DSSP	0.911	0.573	0.929	0.532	0.909	0.347
GraphSite	0.915	0.589	0.934	0.544	0.917	0.369

Note: AF2 Single denotes the single representation produced by AlphaFold2, and Evo denotes the evolutionary feature groups PSSM and HMM. Bold fonts indicate the best results.

Table 3. Performance comparison of GraphSite with state-of-the-art methods on Test_129 and independent Test_181

Dataset	Method	Spe	Rec	Pre	F1	MCC	AUC	AUPR	P-values of AUPR
Test_129	SVMnuc	0.966	0.316	0.371	0.341	0.304	0.812	0.302	6.6×10^{-14}
	NCBRPred	0.969	0.312	0.392	0.347	0.313	0.823	0.310	2.2×10^{-11}
	DNAPred	0.954	0.396	0.353	0.373	0.332	0.845	0.367	2.3×10^{-11}
	COACH-D ^a	0.958	0.367	0.357	0.362	0.321	0.710	0.269	2.7×10^{-11}
	NucBind ^a	0.966	0.330	0.381	0.354	0.317	0.811	0.294	9.2×10^{-12}
	DNABind ^a	0.926	0.601	0.346	0.440	0.411	0.858	0.402	1.9×10^{-10}
	GraphBind ^a	0.941	0.684	0.422	0.522	0.500	0.928	0.519	6.1×10^{-5}
	COACH-D ^b	0.955	0.328	0.318	0.323	0.279	0.712	0.248	3.1×10^{-11}
	NucBind ^b	0.964	0.322	0.366	0.343	0.304	0.809	0.284	8.0×10^{-13}
	DNABind ^b	0.952	0.487	0.389	0.433	0.395	0.832	0.391	1.1×10^{-11}
	GraphBind ^b	0.948	0.625	0.434	0.512	0.484	0.916	0.497	2.6×10^{-7}
	GraphSite	0.950	0.665	0.460	0.543	0.519	0.934	0.544	N/A
Test_181	NCBRPred	0.964	0.259	0.241	0.250	0.215	0.771	0.183	7.2×10^{-11}
	SVMnuc	0.960	0.289	0.242	0.263	0.229	0.803	0.193	7.1×10^{-11}
	DNAPred	0.948	0.334	0.223	0.267	0.233	0.802	0.230	6.2×10^{-10}
	COACH-D ^a	0.971	0.254	0.280	0.266	0.235	0.655	0.172	2.8×10^{-12}
	NucBind ^a	0.960	0.293	0.248	0.269	0.234	0.796	0.191	7.6×10^{-11}
	DNABind ^a	0.904	0.535	0.199	0.290	0.279	0.825	0.219	4.6×10^{-10}
	GraphBind ^a	0.933	0.624	0.293	0.399	0.392	0.904	0.339	3.9×10^{-5}
	COACH-D ^b	0.971	0.239	0.266	0.251	0.220	0.668	0.169	3.4×10^{-12}
	NucBind ^b	0.959	0.288	0.240	0.262	0.227	0.798	0.186	5.5×10^{-11}
	DNABind ^b	0.941	0.392	0.229	0.289	0.259	0.803	0.208	2.8×10^{-10}
	GraphBind ^b	0.949	0.505	0.304	0.380	0.357	0.893	0.317	7.4×10^{-7}
	GraphSite	0.958	0.517	0.354	0.420	0.397	0.917	0.369	N/A

Note: The results of GraphBind were obtained from its standalone program, while the predictions by other competitive methods were generated from their web servers. Bold fonts indicate the best results. ^aUsing native protein structures. ^bUsing predicted protein structures.

that use native protein structures. On the other hand, when using predicted structures as input, our method surpasses the best structure-based method GraphBind by 16.4% in AUPR and 11.2% in MCC, respectively. This suggests that our method is practical and much more powerful for the situation where only protein sequences instead of native structures are available.

Impact of the quality of predicted protein structure

Since GraphSite employs predicted protein structures for geometric deep learning, the predicted quality of AlphaFold2 should be crucial to the downstream DNA-binding site prediction. We calculated the average global distance test (GDT; [62]) between the native structures and the predicted structures by AlphaFold2 in the three datasets through SPAlign [63]. The average GDT for Train_573 and Test_129 are 0.86 and 0.85, indicating that AlphaFold2 can make accurate structure predictions when similar structure templates are available. However,

the predicted quality drops when we set the restriction of the max available date of templates in AlphaFold2. Concretely, the GDT drops to 0.71 for the independent Test_181, which partly explains why the performance of GraphSite decreases in this dataset. For further demonstration, Figure 4 shows the predicted quality (measured by GDT) of AlphaFold2 and the per-protein AUPR on Test_181 for GraphSite (blue scatters). Moreover, we sorted the proteins in Test_181 according to the GDT and divided them into nine bins equally to compute the average GDT and AUPR for each bin (red line). As expected, GraphSite shows a positive correlation between the predicted quality of AlphaFold2 and the AUPR. A closer inspection shows that the top-30% proteins with the highest GDT (average GDT=0.92) correspond to an average AUPR of 0.525 predicted by GraphSite. On the other hand, the bottom-30% proteins with the lowest GDT (average GDT=0.46) correspond to an average AUPR of 0.287, which is significantly lower than that of the top-30% proteins (P -value = 9.0×10^{-5}).

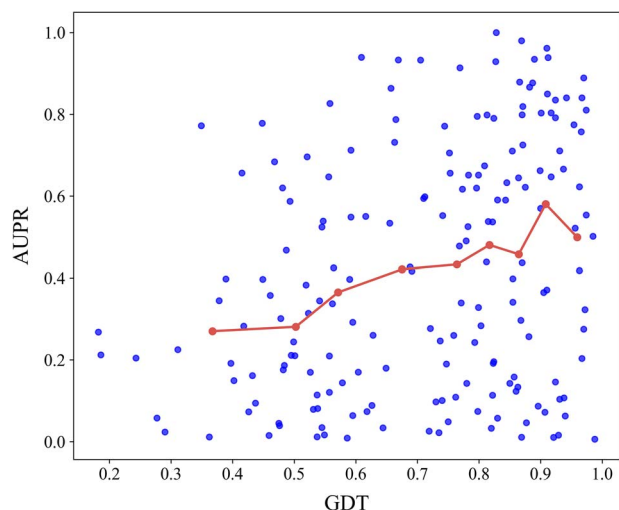


Figure 4. The positive correlation between the predicted quality of AlphaFold2 measured by GDT and the performance of GraphSite measured by AUPR on Test_181. The blue scatters denote the per-protein GDT and AUPR, while the red line denotes the average GDT and AUPR for each bin after sorting all proteins according to GDT and dividing them into nine bins.

according to Mann–Whitney *U* test [64]. We also observed a negative correlation between the predicted error of AlphaFold2 at amino acid level (measured by the distance between the native and predicted amino acid after structure alignment) and the performance of GraphSite (Supplementary Table S5). These results suggest the importance of the predicted quality of protein structure for DNA-binding site prediction.

GraphSite learns effective latent representations of residues

In this section, we visualized the raw feature vectors and the latent feature vectors learned by GraphSite on Test_181. For a target residue, the initial node feature vector consisting of MSA information and structural properties with the size of 438 serves as the raw feature vector. The latent feature vector learned by GraphSite with the size of 128 is the concatenation of the embedding vectors from the two-graph transformer layers. t-SNE [65] was applied to project the high-dimensional feature vectors into the two-dimensional space. Figure 5A and B illustrate the distributions of samples encoded by raw feature vectors and latent feature vectors, respectively. As shown in Figure 5A, the binding and non-binding residues overlap and are indistinguishable, whereas Figure 5B shows that most binding residues are clustered together and separated from most non-binding residues. These results demonstrate that the latent representations learned by GraphSite effectively improve the discriminability of binding and non-binding residues.

Case study

To visualize the superiority of our method, we selected mycobacterial DNA polymerase LigD (PDB ID: 6SA0, chain A) from Test_181 for illustration. Figure 6 shows

the DNA-binding site prediction results of GraphSite (A) and the geometric-agnostic baseline method BiLSTM (B). In this example, there are 32 DNA-binding residues over a total of 333 residues. GraphSite predicts 48 binding residues in which 24 are TP, leading to an F1 of 0.600, MCC of 0.562 and AUPR of 0.554. By comparison, BiLSTM predicts 52 binding residues in which only 20 are TP, leading to a lower F1 of 0.476, MCC of 0.421 and AUPR of 0.367. Besides, as shown in Figure 6A, the false-positive binding residues (colored in red) predicted by GraphSite are mostly around the interface of protein–DNA interaction or close to the DNA structure. In addition, the results of the structure-based method GraphBind using the predicted structure of this protein can be found in Supplementary Figure S3. Visualization of another case (PDB ID: 6YMW, chain B) can also be found in Supplementary Figure S4.

Discussion and conclusion

Identifying protein–DNA binding sites is crucial for understanding biological activities and designing novel drugs. Existing sequence-based methods only consider contextual features of the sequential neighbors, leading to their limited predictive performance, while the structure-based methods are not applicable to most proteins that do not have known tertiary structures. Trained with the predicted structure models and the single representations from AlphaFold2, GraphSite achieves great performance (surpassing the best structure-based method) using only protein sequences, which simultaneously solves the limitations of the current sequence-based and structure-based methods. The graph transformer technique adopted by GraphSite is able to refine the geometric characteristics by taking the local structural context topology into account, while most of the competitive methods first extract structural characteristics and then feed these features into some supervised classifiers, separating the feature engineering and classification. In summary, the superiority of GraphSite benefits from two aspects: (i) the predicted structures from AlphaFold2 are of high quality and the single representations are informative and (ii) the structure-aware graph transformer is an effective algorithm to learn the patterns for binding residue prediction.

With the development of sequencing techniques, many DNA-binding proteins have been detected, and such discoveries require confirmations in biological experiments. Since the whole chain screening is time-consuming and expensive, the predictive methods can help narrow down potential binding sites, as indicated in our previous collaborative study [10] to validate nucleic acid binding residues in JAK2 kinase through computational predictions and wet experiments. On the other hand, these predictions can also provide hypotheses and insights for the mechanisms of many disease-causing gene mutations, such as the THOC2

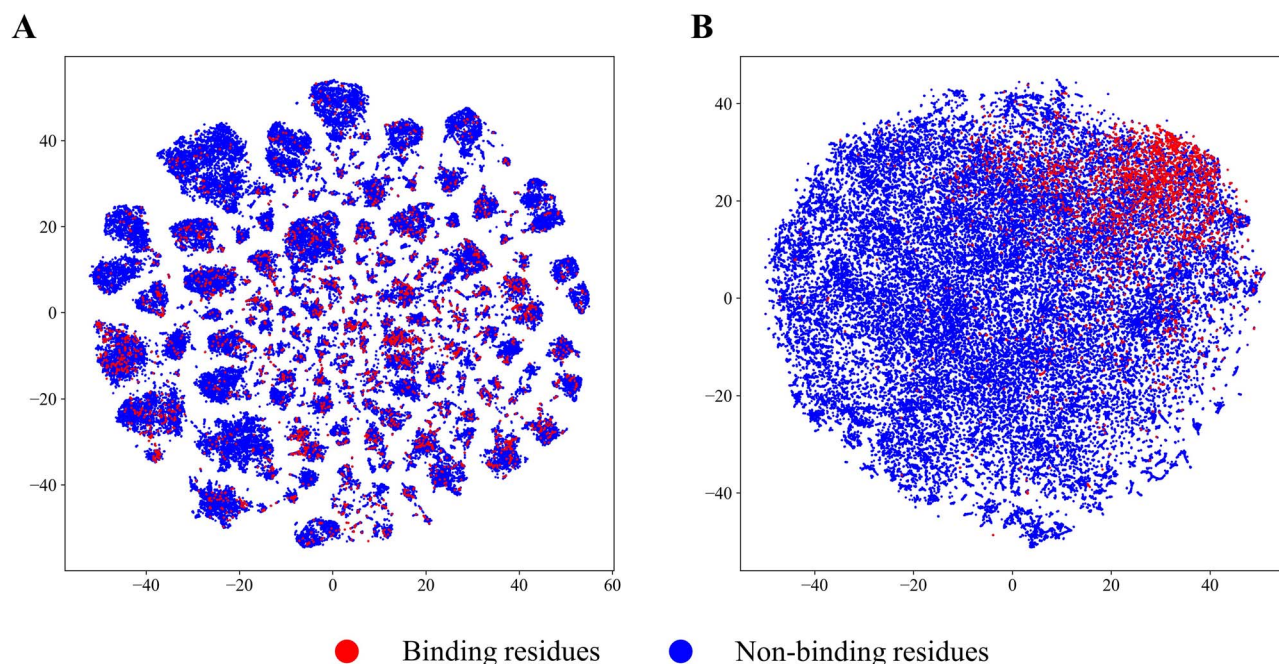


Figure 5. Visualization of the distributions of samples encoded by raw feature vectors (A) and latent feature vectors learned by GraphSite (B) on Test_181 using t-SNE.

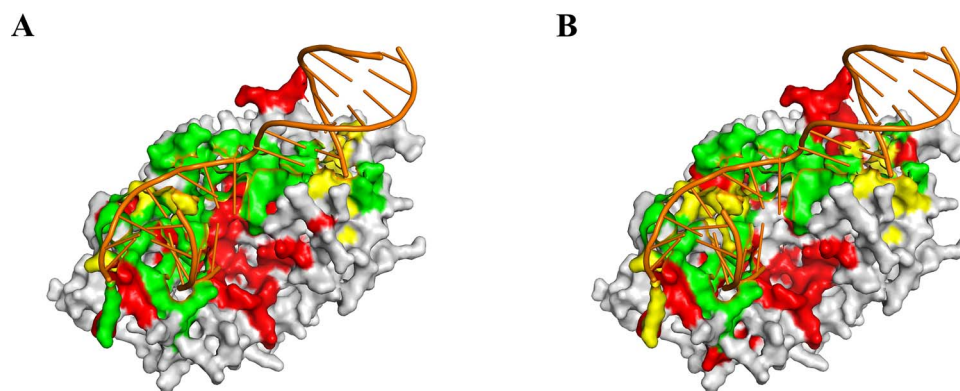


Figure 6. Visualization of one example (PDB ID: 6SA0, chain A) from Test_181 predicted by GraphSite (A) and the geometric-agnostic baseline method BiLSTM (B). TP, FP and FN are colored in green, red and yellow, respectively.

mutations which affect mRNA export [9]. In novel drug design, the binding site prediction can be used to predict druggability [13] or used as condition of generative models for de novo molecule design [14].

Our GraphSite model still has a few limitations. First, the performance of GraphSite is largely affected by the predicted quality of AlphaFold2. This may be solved by adding other informative sequence-derived features or building heterogeneous graphs through integrating protein primary sequences to increase the model robustness to structure predicted quality. Another way is to keep all five-relaxed models from AlphaFold2 instead of only retaining the model with the highest predicted LDDT score to perform data augmentation. Second, our graph transformer algorithm only uses the protein distance matrices as masks in the self-attention step now, and modifications might be made to add the pairwise residue distances as biases to the attention scores. Our

framework can also be explored to handle protein graphs with edge features constructed by residue distance, angle or the pair representation from AlphaFold2. Third, our method only considers the protein information to predict potential DNA-binding sites, thus cannot predict the specific binding pattern given a known DNA sequence or structure. We left these above improvements of this longstanding challenge to future work.

In conclusion, this study proposes a geometric-aware framework called GraphSite for DNA-binding site prediction, where we predict protein structures from sequences using AlphaFold2 and employ graph transformer network to learn the amino acid representations. GraphSite shows preferable performance than other sequence-based and structure-based methods in comprehensive evaluations. We suggest that our method could provide useful information for biologists studying protein-DNA binding patterns or pathogenic mechanisms of

mutations, and chemists interested in targeted drug design. In the future, we would further improve our graph transformer architecture and integrate multi-task learning [66] to extend our method to various fields, including predicting protein binding sites with RNA and small ligands, or protein functional sites such as methylation and phosphorylation.

Key points

- Existing sequence-based methods for identifying protein–DNA binding sites only consider contextual features of the sequential neighbors, which are limited to capture spatial information.
- GraphSite is the first sequence-based method to predict protein–DNA binding sites based on the predicted structures from AlphaFold2, where structure-aware graph transformer is employed to capture the protein structural context topology.
- GraphSite shows preferable performance than state-of-the-art sequence-based and structure-based methods in two independent datasets.

Data availability

We provide the datasets, the predicted structures, and the source codes along with the pre-trained models of GraphSite at <https://github.com/biomed-AI/GraphSite>. The GraphSite web server is freely available at <https://biomed.nscg.cn/apps/GraphSite>.

Supplementary data

Supplementary data are available online at <https://academic.oup.com/bib>.

Acknowledgments

The authors are grateful to Wei Lu and Jixian Zhang from the Galixir Technologies Ltd for providing partial codes. The authors are also much indebted to the three anonymous reviewers, whose constructive comments are helpful for strengthening this paper.

Funding

This study has been supported by the National Key R&D Program of China (2020YFB0204803), National Natural Science Foundation of China (61772566, 62041209), Guangdong Key Field R&D Plan (2019B020228001, 2018B010109006), Introducing Innovative and Entrepreneurial Teams (2016ZT06D211) and Guangzhou S&T Research Plan (202007030010).

Conflict of Interest

This work is done when J.R. works as an intern in Galixir, and S.Z. also currently works directly or indirectly for Galixir.

References

1. Zhao H, Yang Y, Zhou Y. Structure-based prediction of DNA-binding proteins by structural alignment and a volume-fraction corrected DFIRE-based energy function. *Bioinformatics* 2010;**26**: 1857–63.
2. Charoensawan V, Wilson D, Teichmann SA. Genomic repertoires of DNA-binding transcription factors across the tree of life. *Nucleic Acids Res* 2010;**38**:7364–77.
3. Dai H, Umarov R, Kuwahara H, et al. Sequence2vec: a novel embedding approach for modeling transcription factor binding affinity landscape. *Bioinformatics* 2017;**33**:3575–83.
4. Rastogi C, Rube HT, Kribelbauer JF, et al. Accurate and sensitive quantification of protein–DNA binding affinity. *Proc Natl Acad Sci* 2018;**115**:E3692–701.
5. Umarov R, Kuwahara H, Li Y, et al. Promoter analysis and prediction in the human genome using sequence-based deep learning models. *Bioinformatics* 2019;**35**:2730–7.
6. Yan Y, Zhang D, Zhou P, et al. HDock: a web server for protein–protein and protein–DNA/RNA docking based on a hybrid strategy. *Nucleic Acids Res* 2017;**45**:W365–73.
7. Su H, Liu M, Sun S, et al. Improving the prediction of protein–nucleic acids binding residues via multiple sequence profiles and the consensus of complementary methods. *Bioinformatics* 2019;**35**:930–6.
8. Ghersi D, Sanchez R. Improving accuracy and efficiency of blind protein–ligand docking by focusing on predicted binding sites. *Proteins* 2009;**74**:417–24.
9. Kumar R, Corbett MA, Van Bon BW, et al. THOC2 mutations implicate mRNA-export pathway in X-linked intellectual disability. *Am J Hum Genet* 2015;**97**:302–10.
10. Wang S, Liang K, Hu Q, et al. JAK2-binding long noncoding RNA promotes breast cancer brain metastasis. *J Clin Invest* 2017;**127**: 4498–515.
11. Bhardwaj N, Lu H. Residue-level prediction of DNA-binding sites and its application on DNA-binding protein predictions. *FEBS Lett* 2007;**581**:1058–66.
12. Konc J, Hodošček M, Ogrizek M, et al. Structure-based function prediction of uncharacterized protein using binding sites comparison. *PLoS Comput Biol* 2013;**9**:e1003341.
13. Schmidtke P, Barril X. Understanding and predicting druggability. A high-throughput method for detection of drug binding sites. *J Med Chem* 2010;**53**:5858–67.
14. Xu M, Ran T, Chen H. De novo molecule design through the molecular generative model conditioned by 3D information of protein binding sites. *J Chem Inf Model* 2021;**61**:3240–54.
15. Orengo CA, Michie AD, Jones S, et al. CATH—a hierarchic classification of protein domain structures. *Structure* 1997;**5**:1093–109.
16. Mandel-Gutfreund Y, Margalit H. Quantitative parameters for amino acid–base interaction: implications for prediction of protein–DNA binding sites. *Nucleic Acids Res* 1998;**26**:2306–12.
17. Wadkins RM. Targeting DNA secondary structures. *Curr Med Chem* 2000;**7**:1–15.
18. Brázda V, Hároníková L, Liao JC, et al. DNA and RNA quadruplex-binding proteins. *Int J Mol Sci* 2014;**15**:17493–517.
19. Ahmad S, Keskin O, Sarai A, et al. Protein–DNA interactions: structural, thermodynamic and clustering patterns of conserved residues in DNA-binding proteins. *Nucleic Acids Res* 2008;**36**:5922–32.
20. Zhu Y-H, Hu J, Song X-N, et al. DNAPred: accurate identification of DNA-binding sites from protein sequence by ensemble hyperplane-distance-based support vector machines. *J Chem Inf Model* 2019;**59**:3057–71.

21. Zhang J, Ghadermarzi S, Katuwawala A, et al. DNAGenie: accurate prediction of DNA-type-specific binding residues in protein sequences. *Brief Bioinform* 2021;**22**.
22. Zhang J, Chen Q, Liu B. NCBRPred: predicting nucleic acid binding residues in proteins based on multilabel learning. *Brief Bioinform* 2021;**22**.
23. Jones S, Shanahan HP, Berman HM, et al. Using electrostatic potentials to predict DNA-binding sites on DNA-binding proteins. *Nucleic Acids Res* 2003;**31**:7189–98.
24. Tsuchiya Y, Kinoshita K, Nakamura H. Structure-based prediction of DNA-binding sites on proteins using the empirical preference of electrostatic potential and the shape of molecular surfaces. *Proteins* 2004;**55**:885–94.
25. Jiménez J, Doerr S, Martínez-Rosell G, et al. DeepSite: protein-binding site predictor using 3D-convolutional neural networks. *Bioinformatics* 2017;**33**:3036–42.
26. Xia Y, Xia C-Q, Pan X, et al. GraphBind: protein structural context embedded rules learned by hierarchical graph neural networks for recognizing nucleic-acid-binding residues. *Nucleic Acids Res* 2021;**49**:e51–1.
27. Liu R, Hu J. DNABind: a hybrid algorithm for structure-based prediction of DNA-binding residues by combining machine learning-and template-based approaches. *Proteins* 2013;**81**:1885–99.
28. Wu Q, Peng Z, Zhang Y, et al. COACH-D: improved protein-ligand binding sites prediction with refined ligand-binding poses through molecular docking. *Nucleic Acids Res* 2018;**46**:W438–42.
29. Nagarajan R, Ahmad S, Michael GM. Novel approach for selecting the best predictor for identifying the binding sites in DNA binding proteins. *Nucleic Acids Res* 2013;**41**:7606–14.
30. Jumper J, Evans R, Pritzel A, et al. Highly accurate protein structure prediction with AlphaFold. *Nature* 2021;1–11.
31. Lam JH, Li Y, Zhu L, et al. A deep learning framework to predict binding preference of RNA constituents on protein surface. *Nat Commun* 2019;**10**:1–13.
32. Zheng S, Li Y, Chen S, et al. Predicting drug-protein interaction using quasi-visual question answering system. *Nat Mach Intell* 2020;**2**:134–40.
33. Kozlovskii I, Popov P. Protein-peptide binding site detection using 3D convolutional neural networks. *J Chem Inf Model* 2021;**61**:3814–23.
34. Yuan Q, Chen J, Zhao H, et al. Structure-aware protein-protein interaction site prediction using deep graph convolutional network. *Bioinformatics* 2022;**38**(1):125–32.
35. Chen J, Zheng S, Zhao H, et al. Structure-aware protein solubility prediction from sequence through graph convolutional network and predicted contact map. *J Cheminfo* 2021;**13**:7.
36. Vaswani A, Shazeer N, Parmar N, et al. Attention is all you need. In: *Advances in Neural Information Processing Systems*. Long Beach, California, USA, 2017, 5998–6008.
37. Devlin J, Chang M-W, Lee K, et al. Bert: Pre-training of Deep Bidirectional Transformers for Language Understanding. In: *Proceedings of the 2019 Conference of the North American Chapter of the Association for Computational Linguistics*. Minneapolis, Minnesota, 2019, p. 4171–86.
38. Zheng S, Rao J, Zhang Z, et al. Predicting retrosynthetic reactions using self-corrected transformer neural networks. *J Chem Inf Model* 2019;**60**:47–55.
39. Chen L, Tan X, Wang D, et al. TransformerCPI: improving compound-protein interaction prediction by sequence-based deep learning with self-attention mechanism and label reversal experiments. *Bioinformatics* 2020;**36**:4406–14.
40. Ingraham J, Garg V, Barzilay R, et al. Generative models for graph-based protein design. *Adv Neural Inf Process Syst* 2019;**32**:15820–31.
41. Chen J, Zheng S, Song Y et al. Learning attributed graph representation with communicative message passing transformer. In: *Proceedings of the Thirtieth International Joint Conference on Artificial Intelligence*. Montreal-themed virtual reality, 2021, p. 2242–8. International Joint Conferences on Artificial Intelligence.
42. Ying C, Cai T, Luo S, et al. Do Transformers Really Perform Badly for Graph Representation? In: *Thirty-Fifth Conference on Neural Information Processing Systems*. Online, 2021. Curran Associates Inc.
43. Yang J, Roy A, Zhang Y. BioLiP: a semi-manually curated database for biologically relevant ligand-protein interactions. *Nucleic Acids Res* 2012;**41**:D1096–103.
44. Berman HM, Westbrook J, Feng Z, et al. The protein data bank. *Nucleic Acids Res* 2000;**28**:235–42.
45. Fu L, Niu B, Zhu Z, et al. CD-HIT: accelerated for clustering the next-generation sequencing data. *Bioinformatics* 2012;**28**:3150–2.
46. Suzek BE, Huang H, McGarvey P, et al. UniRef: comprehensive and non-redundant UniProt reference clusters. *Bioinformatics* 2007;**23**:1282–8.
47. Mitchell AL, Almeida A, Beracochea M, et al. MGnify: the microbiome analysis resource in 2020. *Nucleic Acids Res* 2020;**48**:D570–8.
48. Steinegger M, Mirdita M, Söding J. Protein-level assembly increases protein sequence recovery from metagenomic samples manyfold. *Nat Methods* 2019;**16**:603–6.
49. Mirdita M, von den Driesch L, Galiez C, et al. Uniclust databases of clustered and deeply annotated protein sequences and alignments. *Nucleic Acids Res* 2017;**45**:D170–6.
50. Steinegger M, Meier M, Mirdita M, et al. HH-suite3 for fast remote homology detection and deep protein annotation. *BMC Bioinform* 2019;**20**:1–15.
51. Altschul SF, Madden TL, Schäffer AA, et al. Gapped BLAST and PSI-BLAST: a new generation of protein database search programs. *Nucleic Acids Res* 1997;**25**:3389–402.
52. Remmert M, Biegert A, Hauser A, et al. HHblits: lightning-fast iterative protein sequence searching by HMM-HMM alignment. *Nat Methods* 2012;**9**:173–5.
53. Kabsch W, Sander C. Dictionary of protein secondary structure: pattern recognition of hydrogen-bonded and geometrical features. *Biopolymers* 1983;**22**:2577–637.
54. Kingma DP, Ba J. Adam: A Method for Stochastic Optimization. In: *3rd International Conference on Learning Representations (Poster)*. San Diego, California, USA: International Conference on Learning Representations, 2015.
55. Paszke A, Gross S, Massa F, et al. Pytorch: an imperative style, high-performance deep learning library. *Adv Neural Inf Process Syst* 2019;**32**:8026–37.
56. Do DT, Le TQT, Le NQK. Using deep neural networks and biological subwords to detect protein S-sulfonylation sites. *Brief Bioinform* 2020;**22**:bbaa128.
57. Le NQK, Ho Q-T, Nguyen T-T-D, et al. A transformer architecture based on BERT and 2D convolutional neural network to identify DNA enhancers from sequence information. *Brief Bioinform* 2021;**22**:bbab005.
58. Saito T, Rehmsmeier M. The precision-recall plot is more informative than the ROC plot when evaluating binary classifiers on imbalanced datasets. *PLoS One* 2015;**10**:e0118432.

59. Yan J, Kurgan L. DRNApred, fast sequence-based method that accurately predicts and discriminates DNA-and RNA-binding residues. *Nucleic Acids Res* 2017;**45**:e84–4.
60. Anderson TW, Darling DA. Asymptotic theory of certain “goodness of fit” criteria based on stochastic processes. *Ann Math Stat* 1952;**23**:193–212.
61. Wilcoxon F. Individual comparisons by ranking methods. *Biometrics* 1945;**1**:80–3.
62. Zemla A. LGA: a method for finding 3D similarities in protein structures. *Nucleic Acids Res* 2003;**31**:3370–4.
63. Yang Y, Zhan J, Zhao H, et al. A new size-independent score for pairwise protein structure alignment and its application to structure classification and nucleic-acid binding prediction. *Proteins* 2012;**80**:2080–8.
64. Mann HB, Whitney DR. On a test of whether one of two random variables is stochastically larger than the other. *Ann Math Stat* 1947;**50**–60.
65. Van der Maaten L, Hinton G. Visualizing data using t-SNE. *J Mach Learn Res* 2008;**9**:2579–605.
66. Sun Z, Zheng S, Zhao H, et al. To improve the predictions of binding residues with DNA, RNA, carbohydrate, and peptide via multi-task deep neural networks. *IEEE/ACM Trans Comput Biol Bioinform* 2021. <https://doi.org/10.1109/TCBB.2021.3118916>.